Progress In Electromagnetics Research C, Vol. 62, 77–87, 2016

Design of a Microstrip-Fed Hexagonal Shape UWB Antenna with Triple Notched Bands

Xun Gong*, Ling Tong, Yu Tian, and Bo Gao

Abstract—In this paper, a microstrip-fed hexagonal shape ultra-wideband (UWB) monopole antenna with triple notched bands is presented. The antenna consists of a microstrip feed line, a regular hexagonal shape radiation patch with a complementary split ring resonator (CSRR) and a pair of inverted T-shaped conductor-backed planes embedded in the antenna backside. Notched bands can be easily controlled by geometry parameters of the CSRR and conductor-backed planes. The simulated and measured results show that this monopole UWB antenna can offer an operation frequency from 2.93 GHz to 10.04 GHz with −10 dB return loss bandwidth, except three notched bands at 3.31–3.78 GHz, 5.33–5.77 GHz and 7.24–7.72 GHz for rejecting the WiMAX and downlink of X-band satellite communication system signals. A good agreement between the measured and simulated results is observed. The proposed antenna provides broadband impedance matching, appropriate gain and stable radiation patterns over its operating bandwidth and can be used in wireless UWB applications.

1. INTRODUCTION

The UWB technology has drawn great attentions in wireless communication applications after the US Federal Communications Commission (US FCC) approved the frequency band from 3.1 GHz to 10.6 GHz for commercial communications [1]. The UWB technology has been used widely in various wireless communication applications because of low cost, low complexity, high data transmission rates, etc. The design of UWB antennas is not easy because the requirements such as omnidirectional radiation pattern, easy manufacture, ultrawide impedance bandwidth, high radiation efficiency, constant gain, etc.

In recent years, lots of UWB antennas have been presented for various applications. The monopole antennas and slot antennas are more suitable candidates for UWB antennas. Printed circular disc monopole antennas fed by microstrip [2] or coplanar waveguide [3] have been studied. Other typical shapes of UWB monopole antennas have been discussed, such as ellipse [4], rectangle [5], hexagon [6] and half-disc [7]. The slot antennas are another focus of UWB antennas. A novel printed microstrip-fed wide-slot antenna with E-shaped patch and E-shaped slot has been proposed in [8]. A compact microstrip-fed UWB tapered-shape slot antenna has been presented in [9]. And a compact hexagonal wide-slot antenna with microstrip-fed monopole has been discussed in [10].

The interference is a problem for UWB communication systems, because there are some other traditional narrow band systems working in the UWB frequency band, such as worldwide interoperability for microwave access (WiMAX, IEEE 802.16) operating at 3.3–3.7 GHz and 5.35–5.65 GHz, wireless local area network (WLAN, IEEE 802.11) operating at 5.15–5.35 GHz and 5.725–5.825 GHz, downlink of X-band satellite communication operating at 7.25–7.75 GHz, dedicated short range communication operating at 5.85–5.925 GHz, etc. To prevent this problem, UWB antennas with band-notched characteristic are necessary. A few different methods have been used to design printed UWB monopole antennas with notched band characteristic. The UWB antennas with band-notched characteristic by

Received 17 October 2015, Accepted 11 January 2016, Scheduled 16 February 2016
* Corresponding author: Xun Gong (gongxunhlj@uestc.edu.cn).
The authors are with School of Automation, University of Electronic Science and Technology of China, Chengdu 611731, China.

etching C-shaped [11], U-shaped [6, 12], meandered-shaped [13] slots on the radiation patch have already been proposed. A compact printed UWB antenna with two notched stop bands by introducing a unit complementary split ring resonator in the beveled edges of the radiating patch has been proposed in [14]. In [15], a printed microstrip-fed monopole UWB antenna with triple notched bands by embedding a modified H-shaped resonator has been presented. In [16], a fork-shaped monopole UWB antenna with a band-notched open-looped resonator has been discussed. A dual band-notched UWB antenna with a pair of conductor-backed planes embedded in the antenna backside has been studied in [17].

In this paper, a hexagonal shape triple band-notched UWB monopole antenna with a CSRR and a pair of inverted T-shaped conductor-backed planes embedded in the backside of the antenna is presented. By adjusting geometry parameters of the CSRR and conductor-backed planes, the notched frequencies can be controlled. The simulated and measured results show that this monopole UWB antenna can offer an operation frequency from 2.93 GHz to 10.04 GHz with -10 dB return loss bandwidth, except three notched bands for rejecting the WiMAX and downlink of X-band satellite communication system signals. The results measured by Agilent Technologies E8363B PNA network analyzer and simulated by the CST Microwave Studio are in good agreement. The proposed antenna can be used in wireless UWB applications.

2. ANTENNA DESIGN

The geometry of the proposed triple band-notched UWB antenna is shown in Fig. 1. In Fig. 1(a) and Fig. 1(b), the top and bottom views of the proposed antenna are shown. In Fig. 1(c), the SRR (split ring resonator) which is the complementary structure of the CSRR etched on the radiation patch is shown. The antenna is printed on a layer of dielectric substance (ROGERS 4350B) with permittivity of $\varepsilon_r = 3.66$, loss tangent of $\tan\delta = 0.004$ and height of $h = 0.51$ mm. The microstrip line, ground plane, radiation patch and inverted T-shaped conductor-backed planes are made by copper with thickness of $t = 35\,\mu$m and conductivity of $\sigma = 5.8 \times 10^7$ S/m. The strip width of the feed line is fixed at $Ws = 1.08$ mm to achieve $50\,\Omega$ impedance [18].

The design initially begins with a regular hexagonal monopole antenna as shown in Fig. 2(a). For estimating the lower band-edge frequency of this printed monopole antenna, the standard formulation for cylindrical monopole antenna has been modified by [19] as

$$f_l(\text{GHz}) = \frac{c}{\lambda} = \frac{72}{(H + r + p) \times k}, \tag{1}$$

where H is the height of the planar monopole antenna, r the effective radius of the equivalent cylindrical monopole antenna, $p = Ls - Lg$ the length of the gap between the upper edge of the ground plane and the lower edge of the radiation patch, and the factor $k = 1.15$ is the empirical value for the effect of dielectric material. The unit of lengths in Eq. (1) is millimeter. With the reference to the structure

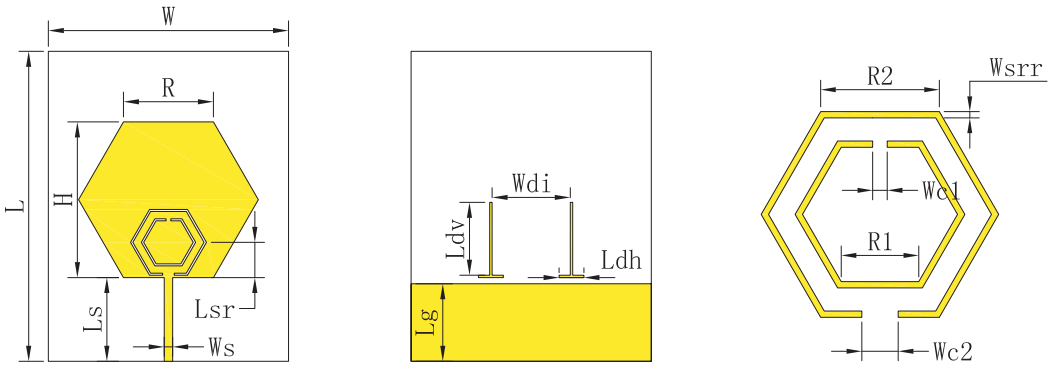

(a) The top view (b) The bottom view (c) The SRR

Figure 1. The geometry of the proposed antenna.

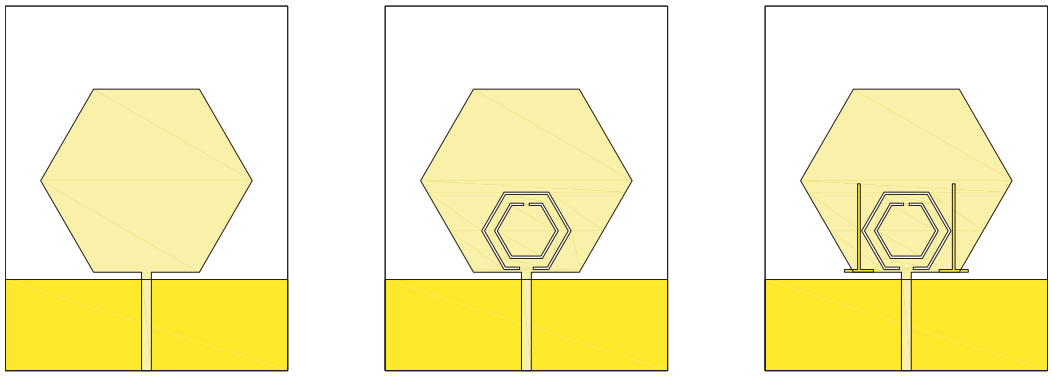

(a) The prototype antenna (b) The prototype antenna with a CSRR (c) The proposed antenna

Figure 2. The structures of the prototype and proposed antennas.

shown in Fig. 1(a), the parameters above can be obtained as follows:

$$H = \sqrt{3}R, \tag{2}$$

$$r = \frac{3R}{4\pi}. \tag{3}$$

By setting the value of $R = 10\,\text{mm}$, parameters of H and r can be calculated by Eqs. (2) and (3). The value of $p = 0.5\,\text{mm}$ can be determined by Eq. (1).

In order to achieve the notched stop bands in the WiMAX band, a unit CSRR is etched in the radiation patch as shown in Fig. 2(b). The characteristics of SRRs and CSRRs have been studied in [20, 21]. The CSRR behaves as an electric dipole that can be excited by an axial electric field. The equivalent lumped-element circuit model of a unit CSRR is a LC resonator with the total capacitance, which can be approximated by parameters of each single slot ring and per unit length inductance between the slot rings. The notched frequency band can be controlled by adjusting the total length of the slot. By slot line theory, the length of each slot in the CSRR can be approximately obtained by

$$L_{notched} = \frac{\lambda_g}{2} = \frac{\lambda_0}{2\sqrt{\varepsilon_{eff}}} = \frac{c}{2f_{notched}\sqrt{\varepsilon_{eff}}}, \tag{4}$$

$$\varepsilon_{eff} \approx \frac{\varepsilon_r + 1}{2}, \tag{5}$$

where λ_g is the guided wavelength, λ_0 the free-space wavelength, ε_{eff} the effective dielectric constant, c the light speed in vacuum, $f_{notched}$ the notched frequency. In this design, the total length of the outer and inner hexagonal-shaped split ring resonators can be obtained by

$$L_{notched\_inner} = 6 \cdot R1 - Wc1, \tag{6}$$

$$L_{notched\_outer} = 6 \cdot R2 - Wc2. \tag{7}$$

The central notched frequencies in the WiMAX band are of $f_{notched\_WiMAX1} = 3.5\,\text{GHz}$ and $f_{notched\_WiMAX2} = 5.5\,\text{GHz}$, so $L_{notched\_outer} = 28.1\,\text{mm}$ and $L_{notched\_inner} = 17.9\,\text{mm}$ can be obtained from Eqs. (4) and (5). By setting the values of $Wc1 = 0.6\,\text{mm}$ and $Wc2 = 1.5\,\text{mm}$, $R1 = 3.08\,\text{mm}$ and $R2 = 4.93\,\text{mm}$ can be calculated by Eqs. (6) and (7).

A pair of inverted T-shaped conductor-backed planes is embedded in the antenna backside for generating the notched band characteristic in downlink of X-band satellite communication system signals band. The inverted T-shaped conductor-backed plane can be considered as a capacitively coupled resonator. The capacitively coupled resonators (such as straight, L-shape, C-shape open-circuited half wavelength resonators or short-circuited quarter wavelength resonators, etc.) have been introduced in antennas for notching band, and the validity is verified [17, 22]. In this design, the inverted T-shaped conductor-backed plane can be approximately considered as a T-shaped printed transmission line resonator with infinite ground plane, and the equivalent diagram is shown in Fig. 3 [23]. For

convenience, the transmission line with the characteristic impedance Z_2 and electrical length θ_2 is chosen as the input port. If either of the two open stubs with the characteristic impedance Z_1 and electrical length θ_1 is chosen as the input port, the same results can be obtained. The input impedance Z_{in} can be analyzed by

$$Z_{in1} = -\frac{Z_1}{2} j \cot\theta_1, \tag{8}$$

$$Z_{in} = Z_2 \frac{Z_{in1} + jZ_2 \tan\theta_2}{Z_2 + jZ_{in1} \tan\theta_2}. \tag{9}$$

While the Wtr of both the strips which compose the T-shaped resonator are fixed to 0.3 mm, and the characteristic impedance $Z_1 = Z_2 = Z$. Eq. (9) can be simplified as

$$Z_{in} = Z \frac{1 - 2\tan\theta_2 \tan\theta_1}{j(2\tan\theta_1 + \tan\theta_2)}. \tag{10}$$

By applying the resonance condition $Z_{in} = \infty$, the resonance condition equation can be obtained as

$$2\tan\theta_1 + \tan\theta_2 = 0. \tag{11}$$

with

$$\theta_1 = \sqrt{\varepsilon_{re}} \cdot k_0 \cdot \frac{Ldh}{2}, \tag{12}$$

$$\theta_2 = \sqrt{\varepsilon_{re}} \cdot k_0 \cdot Ldv, \tag{13}$$

$$k_0 = 2\pi f_{notched} \cdot \sqrt{\varepsilon_0 \mu_0}, \tag{14}$$

where ε_{re} is the effective dielectric constant of the equivalent microstrip lines with the infinite length in each open stub, $f_{notched}$ the notched frequency, ε_0 the dielectric constant of vacuum, and μ_0 the permeability of vacuum. The central notched frequency of X-band satellite communication system is $f_{notched\_Xband} = 7.5$ GHz. The characteristic impedance Z and effective dielectric constant ε_{re} of the transmission lines can be approximately calculated by the equations in [18]. By setting the parameter value of $Ldh = 3$ mm, $Ldv = 9.7$ mm is obtained.

Finally, because the effects of some factors (such as the interactions between the CSRR and T-shaped conductor-backed planes, approximate conditions, etc.), the parameters are adjusted by simulation results of CST Microwave Studio. The optimized values of parameters are shown in Table 1, and the simulated results are shown in Fig. 4. The UWB antenna with triple notched bands is obtained. The upper operation frequency is changed from 10.93 GHz to 10.04 GHz, because the structures of CSRR and T-shaped conductor-backed planes near the feed line cause the impedance mismatch.

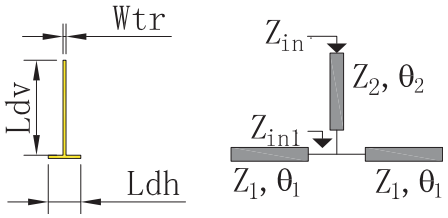

Figure 3. The T-shape resonator and the equivalent diagram.

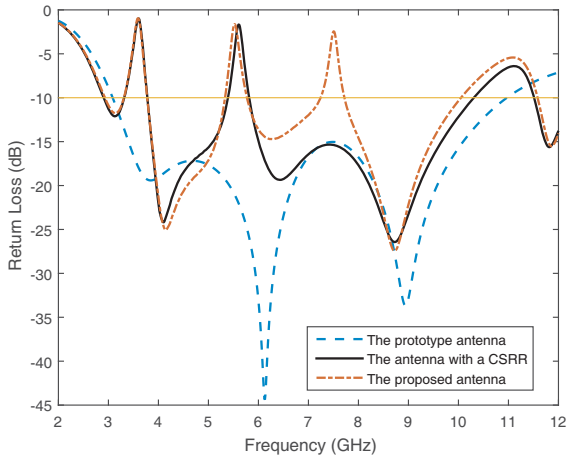

Figure 4. The simulated return losses of the three antennas shown in Fig. 2(c).

Table 1. Optimized parameter of the proposed antenna.

Param.	(mm)	Param.	(mm)	Param.	(mm)	Param.	(mm)
W	31	L	40	Ws	1.08	Ls	10.8
Lg	10	R	11.6	$R1$	3.35	$R2$	4.75
$Wc1$	0.6	$Wc2$	1.5	Lsr	4.55	Ldh	3.2
Ldv	9.7	Wdi	10.4	$Wsrr$	0.3	Wtr	0.3

3. PARAMETRIC STUDY

In this section, the parametric studies are carried out for examining the effects of the important parameters by the CST Microwave Studio. For studying the characteristics of the radiation patch, there are two important parameters, which are the radius (equal to the side length R of the hexagonal patch) of the radiation patch and the gap length $p = Ls - Lg$ between the ground plane and the patch. The simulation model is the prototype antenna shown in Fig. 2(a). The simulated results of different patch radii R are shown in Fig. 5. With increasing radius of the patch, the lower operating frequency decreases because the current path on the patch is extended. The reason can also be found in Eq. (1). The variety of the upper operating frequency caused by the patch radius R may be due to the impedance mismatch and can be adjusted by other parameters such as gap length p. The main effect of the patch radius R is for changing the lower operating frequency. From the simulated results of different gap lengths p as shown in Fig. 6, it is observed that the gap length p has an effect on the impedance matching between the feed line and the radiation patch in the whole band.

The proposed antenna shown in Fig. 2(c) is chosen as the simulation model for studying the characteristics of the CSRR and the T-shaped conductor-backed planes. The inner slot is discussed for the CSRR, because the characteristics of the split ring slots are similar. In the CSRR, the central frequency of notch band can be approximately calculated by Eq. (4). The central frequency $f_{notched\_WiMAX2}$ of the notch band around 5.5 GHz moves rightwards with increasing parameter $Wc1$ and other notched-bands unchanged as shown in Fig. 7. Fig. 8 shows the simulated results of different inner split ring slot radii $R1$. With fixed values of other parameters, the central frequency $f_{notched\_WiMAX2}$ is obviously changed while the split ring slot radius $R1$ is increased, and the central frequency $f_{notched\_WiMAX1}$ of notch band around 3.5 GHz is slightly changed due to the coupling between the inner and outer split ring slots. In Fig. 9, it is observed that both the central frequencies $f_{notched\_WiMAX1}$

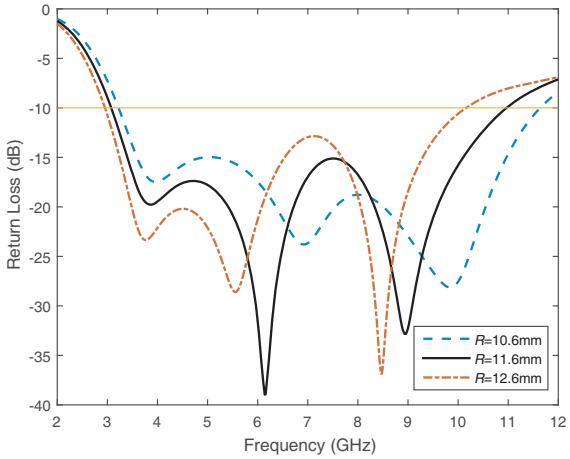

Figure 5. The return losses of different patch radii R.

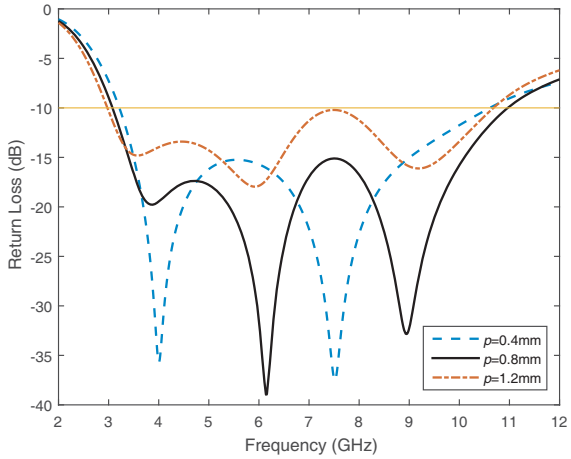

Figure 6. The return losses of different gap lengths p.

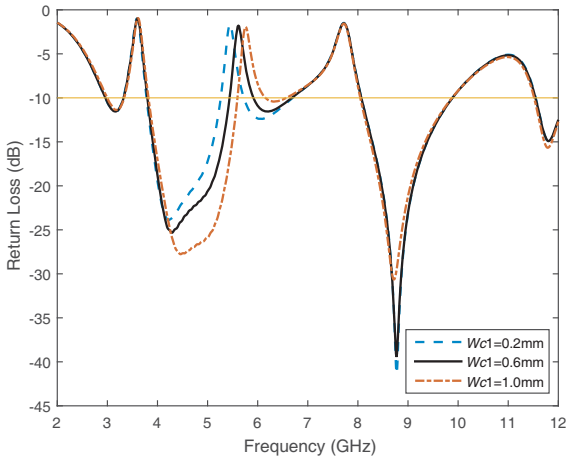

Figure 7. The return losses of different gap widths $Wc1$ on inner split ring slot.

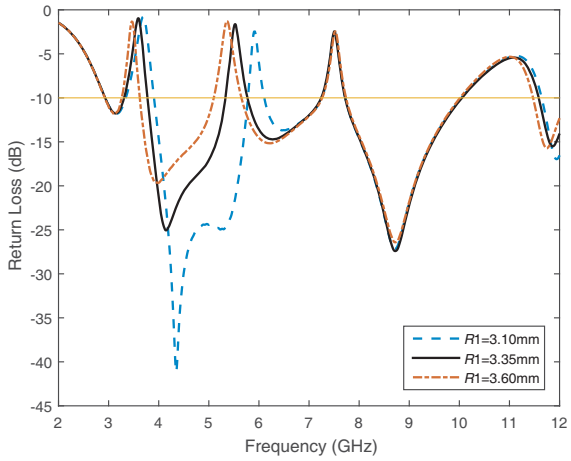

Figure 8. The return losses of different inner split ring slot radii $R1$.

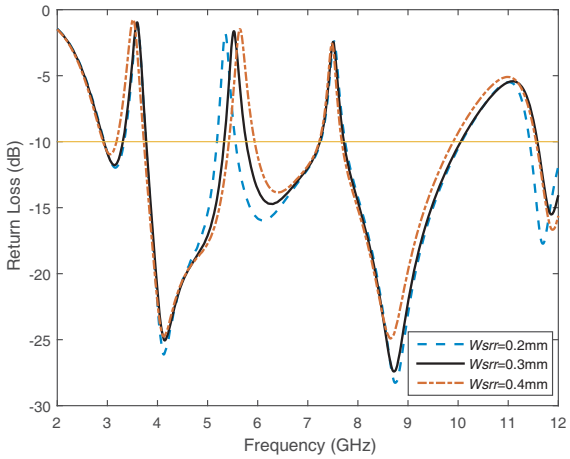

Figure 9. The return losses of different split ring slot widths $Wsrr$.

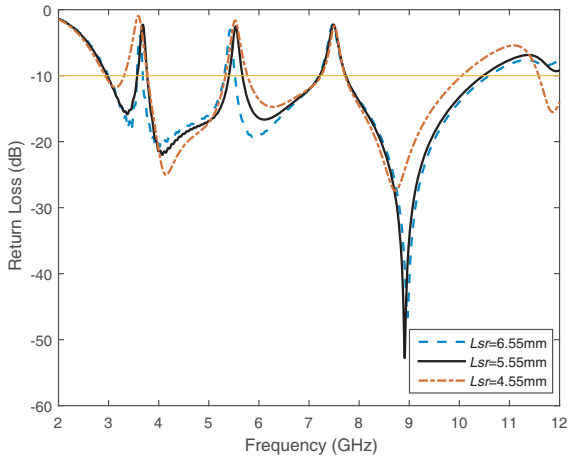

Figure 10. The return losses of different positions Lsr of the CSRR.

and $f_{notched\_WiMAX2}$ are changed with different values of split ring slot widths $Wsrr$, because the equivalent capacitance and inductance of the CSRR are changed with variation of parameter $Wsrr$. While parameter Lsr decreases, the notched bandwidths and the peak values of the return losses at the central frequencies $f_{notched\_WiMAX1}$ and $f_{notched\_WiMAX2}$ are increased with the notched bands moving slightly as shown in Fig. 10, which can be explained by the electromagnetic coupling theory. From the study of the CSRR, the notched bands generated by the CSRR can be controlled by the geometry parameters. The main factors for shifting the central frequencies of notched bands are the lengths and widths of the slots, and the lengths of the slots are more convenient parameters for controlling the central frequencies of notch bands. The central frequencies $f_{notched\_WiMAX1}$ and $f_{notched\_WiMAX2}$ of notched bands can be adjusted independently by the two split ring slots of the CSRR with no effects on the notched band at 7.5 GHz.

Furthermore, the inverse T-shaped conductor-backed planes can be considered as a resonator, and the resonance condition equation is given in Eq. (11). Widths Wtr of the three open stubs in the T-shaped resonator have slight effect on the effective dielectric constant ε_{re} [18], so they have slight effect on the electrical lengths of θ_1 and θ_2. Observing Eqs. (12) and (13), θ_1 and θ_2 are mainly controlled by the lengths of Ldv and Ldh, so the resonance frequency of the T-shaped resonator is mainly controlled by the lengths of Ldv and Ldh. From Fig. 11, it is observed that the central frequency $f_{notched\_Xband}$

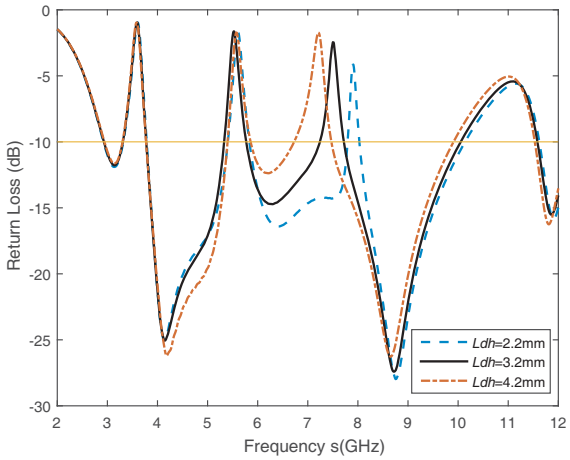

Figure 11. The return losses of different lengths *Ldh* in T-shape resonator.

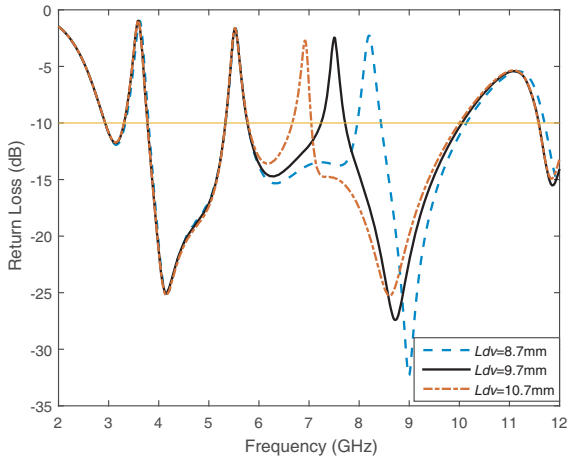

Figure 12. The return losses of different lengths *Ldv* in T-shape resonator.

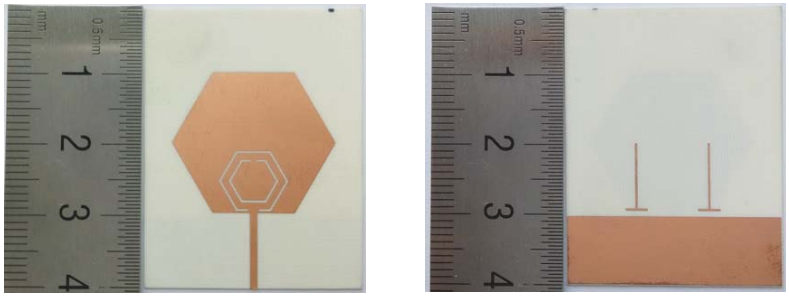

(a) The top view (b) The bottom view

Figure 13. The photograph of the proposed antennas.

of the notch band around 7.5 GHz moves leftwards, and the peak value of the return losses increases while parameter *Ldh* increases. At the same time, the bandwidth of the notched band increases with increasing parameter *Ldh*. And from Fig. 12, it is observed that the central frequency $f_{notched\_Xband}$ moves leftwards with increasing length *Ldv*. From Fig. 11 and Fig. 12, a better way to design the T-shaped conductor-backed planes is first choosing the value of *Ldh* for a suitable peak value of the return loss and bandwidth of the notched band, and then adjusting the value of *Ldv* for a suitable central frequency. The central frequency $f_{notched\_Xband}$ can be adjusted with no effects on the notched bands generated by the CSRR.

4. RESULTS AND DISCUSSION

Photographs of the proposed antenna fabricated based on the design parameters are shown in Fig. 13. In order to measure the antenna frequency response, the Agilent Technologies E8363B PNA network analyzer with the 85056D 2.4 mm economy calibration kit is used. The microstrip feed line of the proposed UWB antenna is connected to the network analyzer through a SMA connector.

The simulated and measured return losses of the proposed antenna are shown in Fig. 14. The fabricated antenna has a frequency band of 3 GHz–10 GHz with three notched-bands around 3.5 GHz, 5.5 GHz and 7.5 GHz. A good agreement between the simulated and measured return losses could be observed. The disagreement may be mainly due to the fabrication tolerance, simulation accuracy and hand welding inaccuracy.

The group delay characteristic is very important in the UWB communications. A pair of proposed

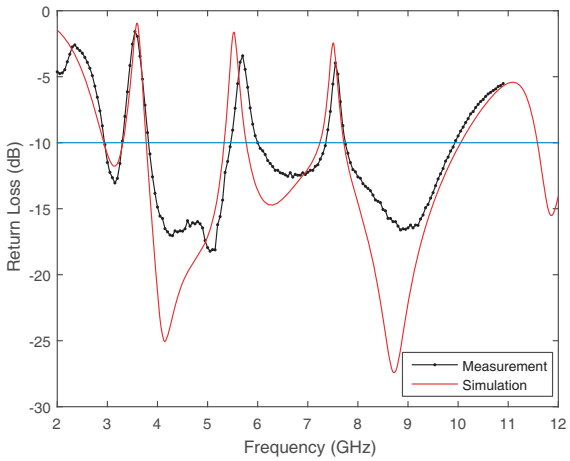

Figure 14. The simulated and measured return losses of the proposed antenna.

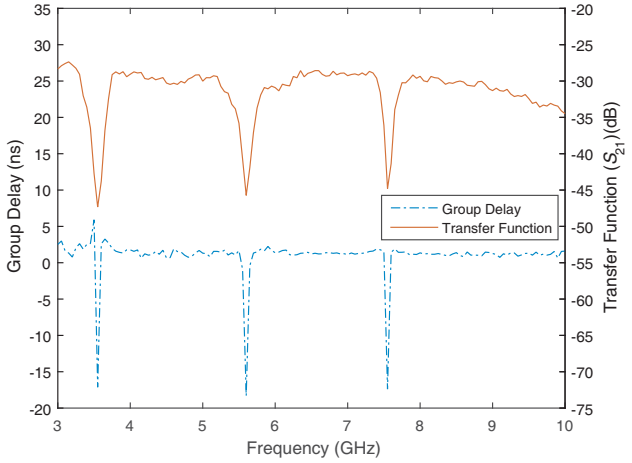

Figure 15. The measured group delay and transfer function of the proposed antenna.

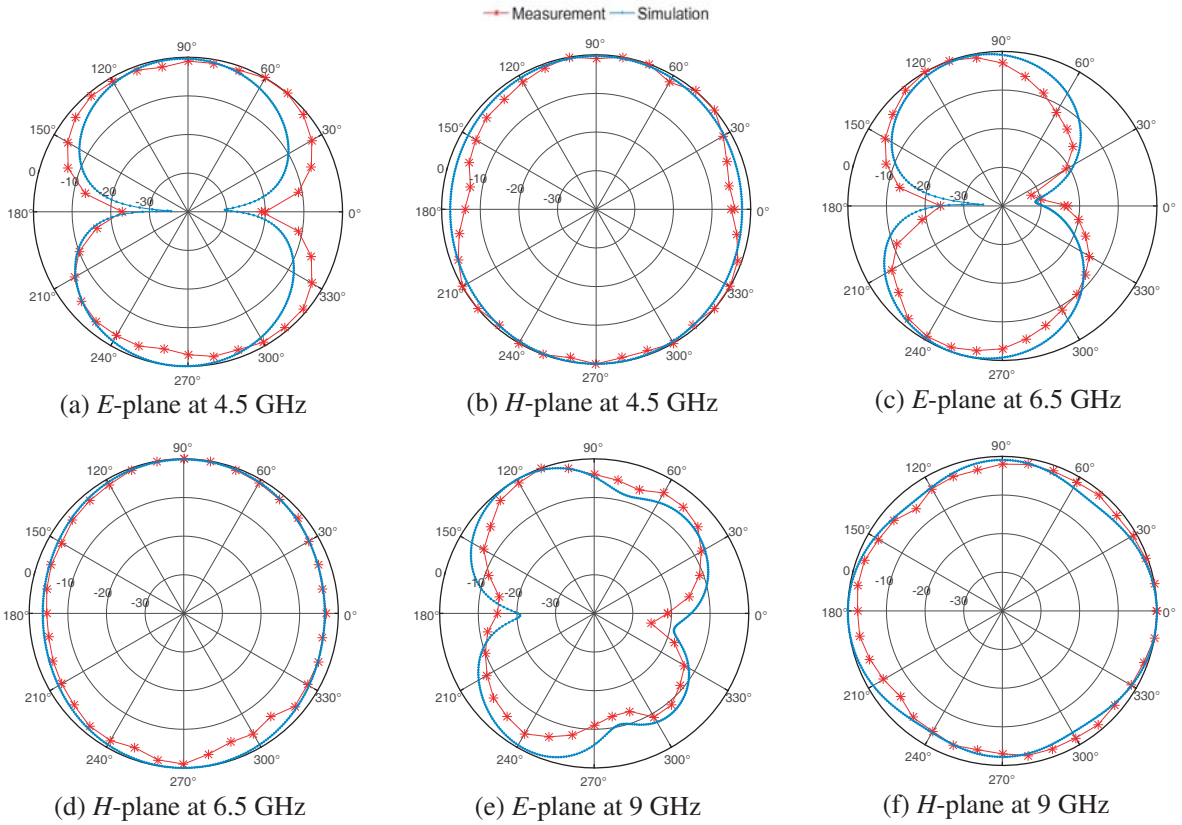

(a) *E*-plane at 4.5 GHz (b) *H*-plane at 4.5 GHz (c) *E*-plane at 6.5 GHz

(d) *H*-plane at 6.5 GHz (e) *E*-plane at 9 GHz (f) *H*-plane at 9 GHz

Figure 16. The radiation patterns of the proposed antenna at 4.5 GHz, 6.5 GHz and 9 GHz.

antennas is used as the transmitting and receiving antennas, and the two antennas are positioned face to face with a distance of 200 mm. The measured result of group delay and the transfer function are shown in Fig. 15. It is observed that the value of group delay is almost constant around 1.5 ns, and the transfer function (S_{21}) is relatively flat in the operation frequency of the proposed antenna except the notched-bands. At the three notched bands, the absolute values of group delay are more than 10 ns. It proves that the proposed antenna has a nearly linear phase response of the transfer function.

Fig. 16 shows the measured and simulated radiation patterns of the proposed antenna in the *E*-

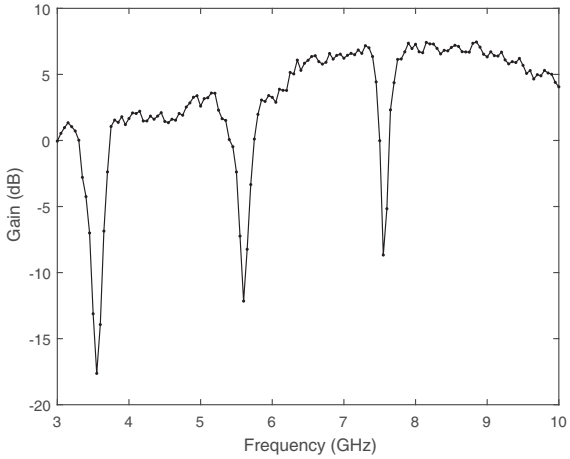

Figure 17. The measured gain of the proposed antenna.

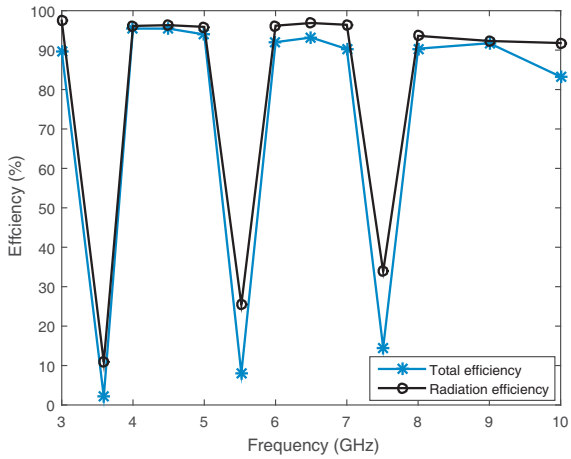

Figure 18. The simulated antenna efficiency of the proposed antenna.

and H-planes at 4.5 GHz, 6.5 GHz and 9 GHz. The measured radiation patterns are very close to the simulated results. It is seen that the radiation patterns of the proposed antenna are omnidirectional in the H-plane at the three frequencies and deteriorate little with the frequency increasing. The radiation patterns in the E-plane are similar to a small electric dipole with bidirectional patterns in a very wide frequency band. The results of Fig. 16 show that the radiation patterns are stable throughout the operation frequency band.

The measured gain is shown in Fig. 17. The gain of the proposed antenna varies from 1.3 to 7.4 dB in the whole operating frequency band except in the notched-bands. The gain value is sufficient and acceptable [6, 17]. Three sharp decreases of the maximum gain in the notched frequency bands at 3.6 GHz, 5.5 GHz and 7.5 GHz is expected. The simulated antenna efficiency characteristics of the proposed antenna, including the total efficiency and radiation efficiency, are shown in Fig. 18. The characteristic can make sure that the proposed antenna can reject the interference effectively [6]. In this design, the total efficiency is more than 83%, and the radiation efficiency is more than 91% over the whole operating frequency band except that the total efficiency is less than 15% and the radiation efficiency less than 34% in the notched-bands.

5. CONCLUSION

In this paper, a microstrip-fed hexagonal shape monopole antenna for UWB applications with triple notched bands is presented. In the proposed antenna, the CSRR and T-shaped conductor-back planes are used for generating the band-notched characteristic. Notched bands can easily be controlled by the geometry parameters of the CSRR and the conductor-backed planes, and these parameters are studied. The simulated and measured results show that this monopole UWB antenna can offer an operation frequency from 2.93 GHz to 10.04 GHz with -10 dB return loss bandwidth, except three notched bands at 3.31–3.78 GHz, 5.33–5.77 GHz and 7.24–7.72 GHz for rejecting the WiMAX and downlink of X-band satellite communication system signals. The measured and simulated results are in good agreement. The proposed antenna provides broadband impedance matching, appropriate gain, linear phase response of the transfer function and stable radiation patterns over its operating frequency bandwidth and can be used in wireless UWB applications.

ACKNOWLEDGMENT

This work is supported by the National Natural Science Foundation of China (Grant No. 61201006).

REFERENCES

1. Federal Communication Commission, "First report and order, revision of part 15 of the commissions rule regarding ultra-wideband transmission systems," Technical report, Washington, DC, Apr. 2002.
2. Liang, J., C. C. Chiau, X. Chen, and C. G. Parini, "Study of a printed circular disc monopole antenna for UWB systems," *IEEE Transactions on Antennas and Propagation*, Vol. 53, No. 11, 3500–3504, Nov. 2005.
3. Liang, J., L. Guo, C. C. Chiau, X. Chen, and C. G. Parini, "Study of CPW-fed circular disc monopole antenna for ultra wideband applications," *IEE Proceedings — Microwaves, Antennas and Propagation*, Vol. 152, No. 6, 520–526, Dec. 2005.
4. Agrawall, N. P., G. Kumar, and K. P. Ray, "Wide-band planar monopole antennas," *IEEE Transactions on Antennas and Propagation*, Vol. 46, No. 2, 294–295, Feb. 1998.
5. Ammann, M. J. and Z. N. Chen, "Wideband monopole antennas for multi-band wireless systems," *IEEE Antennas and Propagation Magazine*, Vol. 45, No. 2, 146–150, Apr. 2003.
6. Mandal, T. and S. Das, "Design of a CPW fed simple hexagonal shape UWB antenna with WLAN and WiMAX band rejection characteristics," *Journal of Computational Electronics*, Vol. 14, No. 1, SI, 300–308, Mar. 2015.
7. Yang, T. and W. A. Davis, "Planar half-disk antenna structures for ultra-wideband communications," *IEEE Antennas and Propagation Society International Symposium, 2004*, Vol. 3, 2508–2511, Jun. 2004.
8. Dastranj, A., A. Imani, and M. Naser-Moghaddasi, "Printed wide-slot antenna for wideband applications," *IEEE Transactions on Antennas and Propagation*, Vol. 56, No. 10, 3097–3102, Oct. 2008.
9. Azim, R., M. T. Islam, and N. Misran, "Compact tapered-shape slot antenna for UWB applications," *IEEE Antennas and Wireless Propagation Letters*, Vol. 10, 1190–1193, Oct. 2011.
10. Ghaderi, M. R. and F. Mohajeri, "A compact hexagonal wide-slot antenna with microstrip-fed monopole for UWB application," *IEEE Antennas and Wireless Propagation Letters*, Vol. 10, 682–685, Jun. 2011.
11. Fakharian, M. M., P. Rezaei, and A. Azadi, "A planar UWB bat-shaped monopole antenna with dual band-notched for WiMAX/WLAN/DSRC," *Wireless Personal Communications*, Vol. 81, No. 2, 881–891, Mar. 2015.
12. Shaalan, A. A. and M. I. Ramadan, "Design of a compact hexagonal monopole antenna for ultra-wideband applications," *Journal of Infrared Millimeter and Terahertz Waves*, Vol. 31, No. 8, 958–968, Aug. 2010.
13. Bialkowski, M. E. and A. M. Abbosh, "Design of UWB planar antenna with improved cut-off at the out-of-band frequencies," *IEEE Antennas and Wireless Propagation Letters*, Vol. 7, 408–410, May. 2008.
14. Sharma, M. M., J. K. Deegwal, M. C. Govil, and Ashok Kumar, "Compact printed ultra-wideband antenna with two notched stop bands for WiMAX and WLAN," *International Journal of Applied Electromagnetics and Mechanics*, Vol. 47, No. 2, 523–532, 2015.
15. Sung, Y., "Triple band-notched UWB planar monopole antenna using a modified H-shaped resonator," *IEEE Transactions on Antennas and Propagation*, Vol. 61, No. 2, 953–957, Feb. 2013.
16. Wu, S.-J., C.-H. Kang, K.-H. Chen, and J.-H. Tarng, "Study of an ultrawideband monopole antenna with a band-notched open-looped resonator," *IEEE Transactions on Antennas and Propagation*, Vol. 58, No. 6, 1890–1897, Jun. 2010.
17. Ojaroudi, Y., S. Ojaroudi, and N. Ojaroudi, "A novel 5.5/7.5 GHz dual band-stop antenna with modified ground plane for UWB communications," *Wireless Personal Communications*, Vol. 81, No. 1, 319–332, Mar. 2015.
18. Collin, R. E., *Foundations for Microwave Engineering*, 2nd Edition, Chapter 3, Wiley-IEEE Press, Dec. 2000.
19. Ray, K. P., "Design aspects of printed monopole antennas for ultra-wide band applications," *International Journal of Antennas and Propagation*, 2008.

20. Baena, J. D., J. Bonache, F. Martin, R. M. Sillero, F. Falcone, T. Lopetegi, M. A. G. Laso, J. Garcia-Garcia, I. Gil, M. F. Portillo, and M. Sorolla, "Equivalent-circuit models for split-ring resonators and complementary split-ring resonators coupled to planar transmission lines," *IEEE Transactions on Microwave Theory and Techniques*, Vol. 53, No. 4, 1451–1461, Apr. 2005.
21. Dissanayake, T. and K. P. Esselle, "Prediction of the notch frequency of slot loaded printed UWB antennas," *IEEE Transactions on Antennas and Propagation*, Vol. 55, No. 11, 3320–3325, Nov. 2007.
22. Lee, W.-S., J.-H. Kim, W.-G. Lim, K.-S. Son, H. S. Lim, and J.-W. Yu, "Capacitively coupled band-stop filter with an integrated antenna," *IEEE MTT-S International Microwave Symposium Digest, 2006*, 2019–2022, Jun. 2006.
23. Bousbia, L., M. Mabrouk, and A. Ghazel, "Study and modeling of T and L shaped resonators for UWB band pass filter," *EUROCON, 2013 IEEE*, 1857–1861, Jul. 2013.